Journal of Power Sources 227 (2013) 185–190

Contents lists available at SciVerse ScienceDirect

Journal of Power Sources

journal homepage: www.elsevier.com/locate/jpowsour

Electrocatalytic activity of nitrogen-doped graphene synthesized via a one-pot hydrothermal process towards oxygen reduction reaction

Jiajia Wu [a,b], Dun Zhang [a,*], Yi Wang [a], Baorong Hou [a]

[a] National Engineering Research Center for Marine Corrosion Protection, Institute of Oceanology, Chinese Academy of Sciences, Qingdao 266071, China
[b] University of the Chinese Academy of Sciences, Beijing 100039, China

HIGHLIGHTS

- Nitrogen-doped graphene (NG) samples with different nitrogen contents are prepared.
- Nitrogen doping favors the reduction of oxygen to water at lower overpotentials.
- Properties of NG are closely related to nitrogen contents and microstructure.
- A nitrogen content of ca. 7% and moderate defect densities provide best activity.

ARTICLE INFO

Article history:
Received 23 August 2012
Received in revised form
7 November 2012
Accepted 21 November 2012
Available online 28 November 2012

Keywords:
Oxygen reduction reaction
Electrocatalysis
Nitrogen-doped graphene
Hydrothermal synthesis

ABSTRACT

Nitrogen-doped graphene (NG) materials have been prepared by hydrothermal reaction of graphite oxide (GO) with urea, and their electrocatalytic properties towards oxygen reduction reaction in 0.1 M KOH are investigated. The introduction of urea leads to successful nitrogen insertion in the form of pyridinic, pyrrolic, and graphitic bonding configurations with enhanced reduction of GO, and an increase in the mass ratio between urea and GO gives higher nitrogen contents, which is accompanied by more defects in microstructure. Reduction of O_2 to OH^- at lower overpotentials is favored by the incorporation of nitrogen, and the activity of NG is closely associated with nitrogen contents and microstructure. NG materials with ca. 7% nitrogen contents and moderate defect densities prepared from mass ratios of 1:200 and 1:300 (GO/urea) show the best performance.

1. Introduction

The alleviation of carbon dioxide poisoning problem by the recent development of anion exchange membrane has revitalized the research interest in alkaline fuel cells (AFCs) [1,2]. Similar to proton exchange membrane fuel cells (PEMFCs), another important low-temperature energy conversion technology, the sluggish kinetics of oxygen reduction reaction (ORR) at the cathode has decreased the energy efficiency of AFCs. Thus, electrocatalysts with high performance are highly desirable. Pt and Pt-based materials are commonly used in PEMFCs owing to their excellent electrocatalytic activity and stability, but more facile kinetics for ORR and less corrosive electrolyte in AFCs make it possible to employ a broader range of electrocatalysts with lower cost [3], such as silver [4], metal oxides [5], metal hydroxides [6], and carbon materials [7]. Among carbon materials reported, graphene with unique physical and chemical properties is attracting more attention.

Graphene possesses good electrocatalytic activity towards ORR in alkaline media, and its modification on glassy carbon (GC) electrode decreases the overpotential and increases the current density [8]. However, the performance of plain graphene hardly meets the practical requirements of AFCs. Therefore, composites of graphene with other electrocatalysts have been developed to give better performance [9–11]. In the meanwhile, chemical doping with foreign atoms is also an effective approach to achieve higher electrocatalytic activity. The heteroatoms mainly refer to nitrogen, boron, and sulfur [12–14], in which nitrogen-doped graphene (NG) has been paid tremendous attention due to its high activity towards ORR. The enhanced ORR performance of NG could be attributed to the alteration of electronic structure, where the electron-accepting ability of nitrogen atoms creates a net positive charge on adjacent

* Corresponding author. Tel./fax: +86 532 82898960.
E-mail addresses: zhangdun@qdio.ac.cn, zhangdun@ms.qdio.ac.cn (D. Zhang).

0378-7753/$ – see front matter © 2012 Elsevier B.V. All rights reserved.
http://dx.doi.org/10.1016/j.jpowsour.2012.11.074

carbon [15]. Much work has been done to investigate the impact of nitrogen content and the proportion of nitrogen species on ORR activity of NG, but the nature of the binding configurations responsible for the enhanced performance is still under discussion [16]. Qu and Yang suggest that pyridinic and pyrrolic nitrogen atoms play an important part in the enhancement of ORR activity [13,14], but Geng insists on the importance of graphitic ones [17]. This divergence may be closely related to different synthesis methods. Furthermore, the role of microstructure in ORR electrocatalytic performance is ignored.

Up to now, several methods have been reported to synthesize NG, including chemical vapor deposition [18], nitrogen plasma treatment [19], arc charge in the presence of nitrogen source vapor [20], and thermal annealing of graphite oxide (GO) with ammonia [21]. These methods are usually complex, require special instruments or rigorous conditions, and do not produce NG at a large scale with low cost, which has prompted researchers to develop facile approaches. Recently, hydrothermal reaction of GO with nitrogen precursors has been viewed as an effective way to synthesize NG with a high nitrogen level [22–25], but the electrocatalytic activity of NG thus obtained towards ORR has not been fully investigated.

In this work, NG materials with different nitrogen contents have been prepared via a one-step hydrothermal reaction of GO and urea with different mass ratios, and their electrocatalytic properties towards ORR in 0.1 M KOH solution have been evaluated. The results show that NG materials enhance the transformation of O_2 to OH^- at lower overpotentials, and their properties are dependent on nitrogen concentrations and microstructure, in which a nitrogen content of ca. 7% and moderate defect densities give the best performance.

2. Experimental

2.1. Synthesis of NG

NG materials were prepared via a one-pot hydrothermal reaction of GO with urea similar to the work of Sun et al. [23]. GO was obtained by a modified Hummers method [26], which contains three steps: pre-oxidation of natural graphite with concentrated H_2SO_4 and $KMnO_4$, re-oxidation with H_2O_2, and exfoliation by sonication. Then, the simultaneous reduction of GO and nitrogen insertion of graphene were achieved by a facile hydrothermal reaction at 170 °C for 12 h, and the nitrogen content and nitrogen species proportion could be readily adjusted by controlling the mass ratio between GO and urea. The mass ratios (GO: urea) used here were 1:100, 1:200, 1:300, 1:400, and 1:500, and corresponding samples obtained were denoted as NG-1, NG-2, NG-3, NG-4, and NG-5. In brief, a given amount of urea was added into 20 mL GO aqueous suspension (1 mg mL^{-1}), and the mixture was ultrasonicated for 2 h. Subsequently, 18 mL mixture was transferred to a Teflon-lined stainless steel autoclave with a volume of 20 mL, sealed and heated. Finally, the resulting product was filtered, washed and dispersed in ethanol. Pure graphene without nitrogen doping was also synthesized by the same method except in the absence of urea.

2.2. Characterization of NG

The chemical composition and state of as-prepared samples were characterized by CHN elemental analysis and X-ray photoelectron spectroscopy (XPS). The former was carried out on a Vario EL III analyzer (Elementar Analysensysteme GmbH), and oxygen content was calculated as the fraction not measured. The latter was performed in an ESCALAB 250 instrument (Thermo Fisher Scientific Inc.) using monochromated Al Kα radiation (1486.6 eV). A Renishaw inVia Raman spectrometer was utilized for microstructure analysis.

Table 1
Chemical composition of different samples. Nitrogen distributions were calculated based on CHN method and XPS measurement. N1 to N4 represent pyridinic, pyrrolic, graphitic type nitrogen, and nitrogen oxide species, respectively.

Sample	Composition (atom %)						
	C	O	N	N1	N2	N3	N4
Graphene	52.25	23.07	0.88	–	–	–	–
NG-1	51.84	16.48	6.05	2.07	2.65	0.81	0.52
NG-2	52.01	16.80	6.78	2.46	2.90	0.94	0.48
NG-3	52.05	16.34	7.25	2.52	3.11	1.12	0.50
NG-4	52.35	16.92	7.28	2.80	2.93	0.98	0.57
NG-5	52.39	16.60	7.65	2.71	3.03	1.34	0.57

2.3. Preparation of modified electrodes and electrochemical measurements

A rotating glassy carbon (GC) disk electrode with a diameter of 5.61 mm was used in this study. Prior to modification, GC electrode was polished with 1.0 and 0.05 μm alumina slurries, and then cleaned in Milli-Q water by sonication for 10 min. To prepare NG

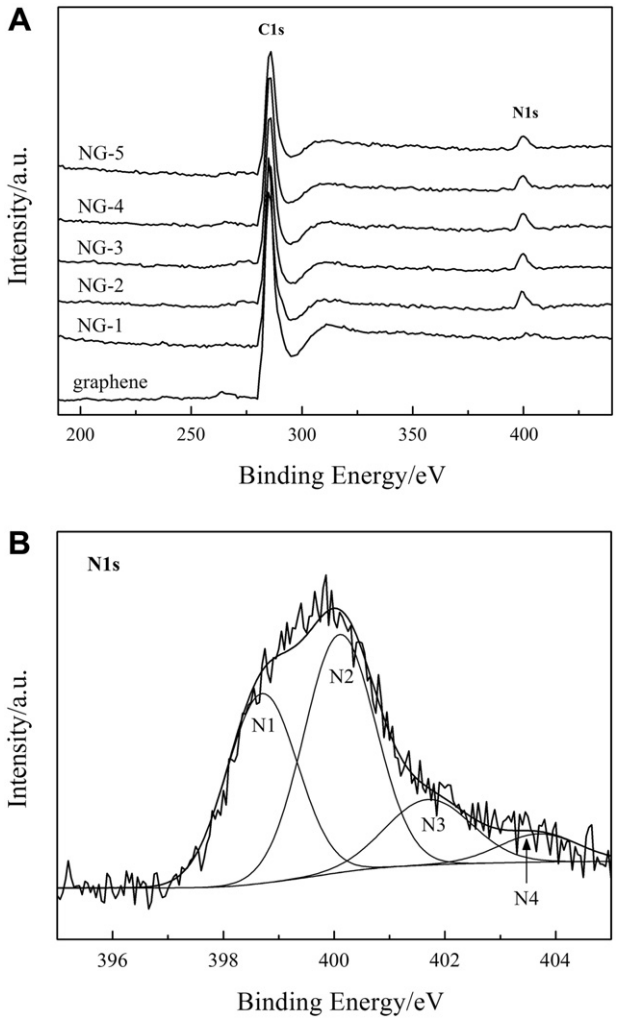

Fig. 1. (A) XPS spectra of different samples. (B) High-resolution N1s spectrum of NG-1. N1 to N4 have the same meanings as described in Table 1.

modified GC (abbreviated as NG/GC) electrodes, 17 μL NG ethanol dispersion with a concentration of ca. 2 mg mL^{-1} was pipetted onto the GC surface and allowed to dry in air, and then 10 μL Nafion ethanol solution (0.05 wt%) was coated and air-dried. For comparison, GC electrodes modified with graphene and commercial Pt/C (46.3% Pt, Tanaka Kikinzoku Kogyo Co. Ltd.) ware also prepared in the same way, which can be abbreviated as graphene/GC and Pt-C/GC electrodes.

Cyclic voltammograms (CVs) and linear sweep voltammograms (LSVs) were recorded on a computer-controlled 760C electrochemical analyzer (CH Instruments, Inc.) in a three-electrode system with 0.1 M KOH as electrolyte. The working electrodes consisted of GC, Pt-C/GC, graphene/GC, and different NG/GC electrodes. A Pt wire and an Ag/AgCl (KCl-sat.) electrode were used as the counter electrode and reference electrode, respectively. All potentials are reported versus the Ag/AgCl (KCl-sat.) electrode, and all experiments were carried out at room temperature (25 °C).

3. Results and discussion

Table 1 lists chemical composition of graphene and different NG materials determined by CHN elemental analysis. Quite a low nitrogen content is obtained in graphene, which mainly originates from the incomplete removal of $NaNO_3$ used in GO preparation. The addition of urea not only results in nitrogen doping, but also enhances the reduction of GO, as can be proved by the decrease of oxygen content in NG. This phenomenon is closely relevant to the slow release of NH_3 from urea during hydrothermal treatment. NH_3 reacts with the oxygen functional groups like carbonyl, carboxyl, and lactone in GO to achieve the insertion of nitrogen [21]. Meanwhile NH_3 can increase the pH of aqueous dispersion to give more effective deoxygenation of GO [27]. Since the proportions of

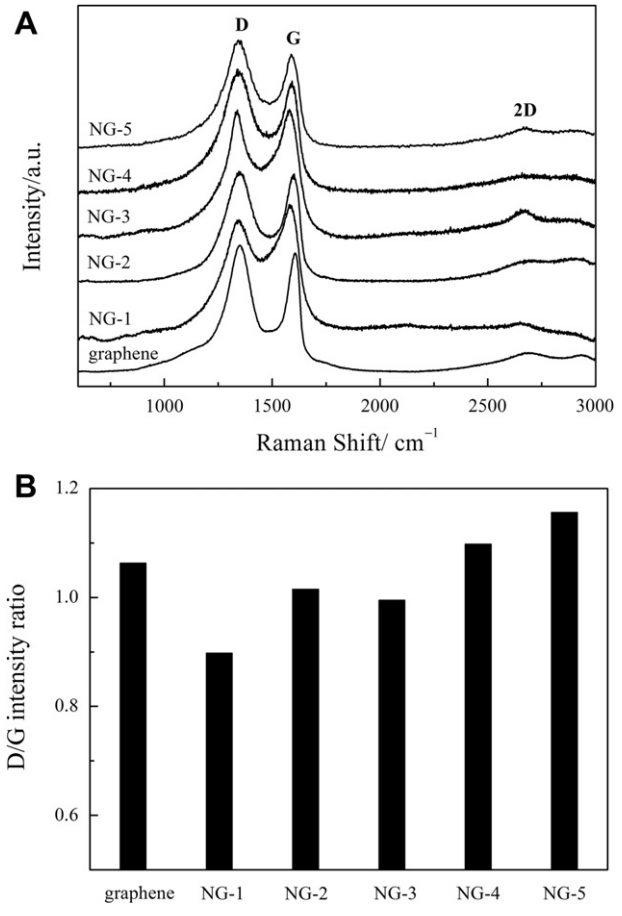

Fig. 2. Raman spectra of different samples. The corresponding D/G intensity ratios are shown in (B).

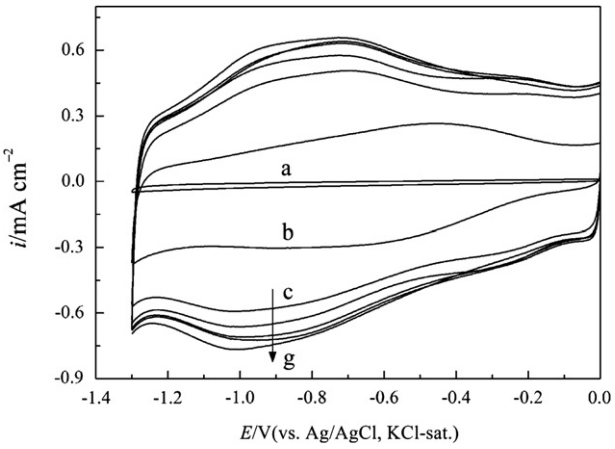

Fig. 3. CVs obtained in N_2-saturated 0.1 M KOH solution at different electrodes (a: GC; b: graphene/GC; c: NG-5/GC; d: NG-4/GC; e: NG-2/GC; f: NG-1/GC; g: NG-3/GC). Scan rate: 50 mV s^{-1}. Current densities are normalized to the geometrical area of GC disk electrode.

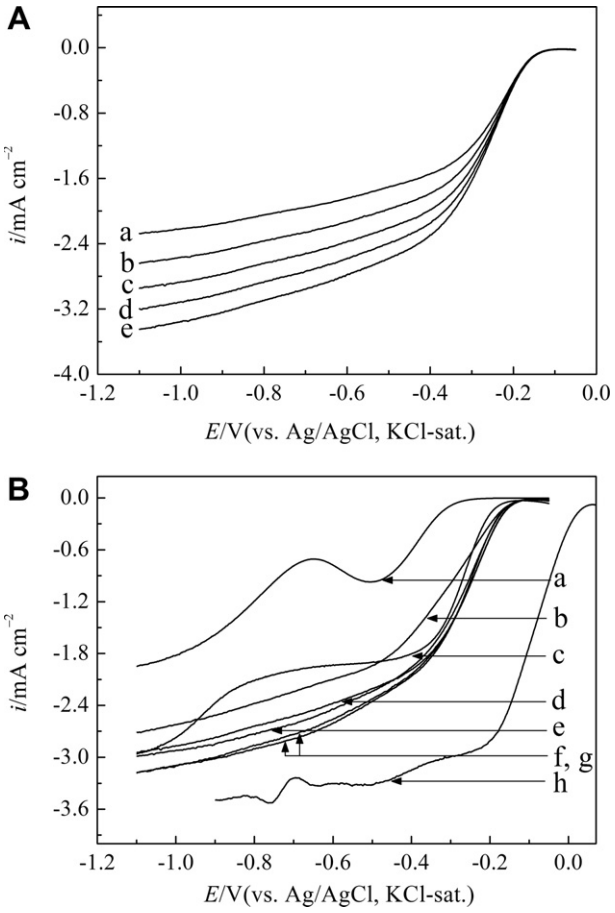

Fig. 4. (A) LSVs recorded on NG-1/GC electrode in O_2-saturated 0.1 M KOH solution at different rotation rates (a: 400; b: 600; c: 800; d: 1000; e: 1200 rpm). (B) Comparison of LSVs for ORR obtained at different electrodes with a rotation rate of 800 rpm. Curves a to h correspond to GC, NG-5/GC, graphene/GC, NG-1/GC, NG-4/GC, NG-2/GC, NG-3/GC, and Pt-C/GC electrode, respectively. Scan rate: 10 mV s^{-1}. All curves are corrected from the blank current under N_2, and current densities are normalized to the geometrical area of GC disk electrode.

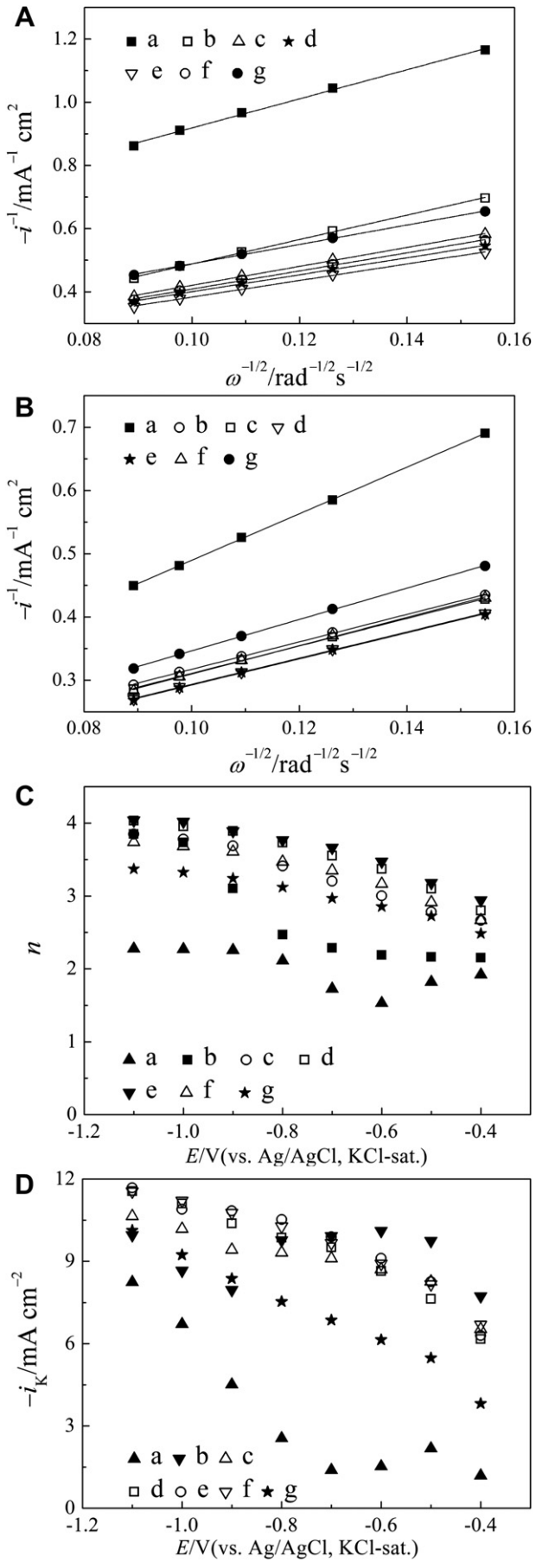

Fig. 5. K–L plots for different electrodes at potentials of −0.5 V (A) and −1.1 V (B). The dependence of n (C) and i_k (D) on potential at different electrodes. Curves a to g refer to GC, graphene/GC, NG-1/GC, NG-2/GC, NG-3/GC, NG-4/GC, and NG-5/GC electrode, respectively.

oxygen in all NG materials are among 16–17%, they have a similar reduction level. As a consequence, a mass ratio of 1:100 is enough for the complete reduction of GO under these conditions. But further increase in the amount of urea improves the nitrogen content from 6.05% of NG-1 to 7.65% of NG-5, which seems to be in conflict with the result of Sun's that a mass ratio of 1:300 gives the highest nitrogen concentration [23]. This difference is associated with diversities in the oxidation state of GO, GO concentration, hydrothermal temperature, and filling degree of autoclaves.

The chemical bonding information of samples characterized by XPS is shown in Fig. 1A. In the spectrum of graphene, a peak around 284 eV assigned to C1s photoelectron excitation is observed. The presence of N1*s* peak around 400 eV in NG materials' spectra demonstrates the successful incorporation of nitrogen, which is in good agreement with the results of CHN elemental analysis. Fig. 1B depicts the typical high-resolution N1*s* spectrum of NG, and the types of nitrogen species and their distribution were identified by the curve-fitting procedure using XPS Peak-fit software. The peaks at 398.7, 400.1, and 401.7 eV that are common in nitrogen-doped carbon materials, correspond to the pyridinic (N1), pyrrolic (N2), and graphitic type nitrogen (N3), respectively [17,24,28–30]. N1 and N2 represent nitrogen atoms bonding with two carbon atoms, and donate one or two *p*-electron to the aromatic π-system. N3, also called "quaternary nitrogen", refers to nitrogen atoms that substitute the carbon atoms in graphene layers [31]. Here, we also introduce a peak at the binding energies of >402 eV for nitrogen oxide species (N4) [32,33], given the fact that a small amount of nitrogen from $NaNO_3$ residue has been detected in graphene by CHN elemental analysis. Although a higher mass ratio between urea and GO leads to a higher total nitrogen content of NG, the proportions of N1, N2, and N3 do not change regularly with the rise in mass ratios. Independent on the ratio between reactants, the contents of N4 are similar in all NG materials, indicating that nitrogen doping from urea is achieved in the form of N1–N3.

Raman spectroscopy is a powerful tool to characterize the structure and quality of graphene. The spectra of all samples exhibit two remarkable peaks located at around 1350 and 1590 cm^{-1} (Fig. 2A), which can be attributed to D band associated with structural defects and G band for E_{2g} vibration mode of *sp*2 carbon domains. The broad peak at around 2700 cm^{-1} demonstrates that the present synthesis method gives few-layer graphene [34,35]. Commonly the intensity ratio of D band to G band (I_D/I_G) reflects the defect density in carbon materials. As can be seen from Fig. 2B, the value of I_D/I_G varies with the mass ratio between reactants. The addition of urea leads to a decrease of I_D/I_G from 1.06 of graphene to 0.90 of NG-1, but further increase in urea concentration brings higher I_D/I_G values, and the values of NG-4 and NG-5 are larger than that of graphene. The defect density is closely relevant to the degree of GO reduction and nitrogen doping. It has been stated in CHN elemental analysis, the addition of urea causes successful insertion of nitrogen with the improvement of GO reduction degree. Nitrogen incorporation and enhancement of GO reduction have opposite effects on defect density, in which the former introduces new defective sites and the latter lowers defect density. When the amount of urea is small, the role of reduction enhancement is prominent. The influence of nitrogen doping is greater in the occasions of high urea concentration, and larger I_D/I_G values are

obtained. The difference in chemical composition and microstructure among these materials will have significant impact on their ORR electrocatalytic properties discussed below.

Fig. 3 displays CVs obtained at different electrodes in N_2-saturated 0.1 M KOH solution. Compared with the bare GC electrode, modification of graphene and NG results in the appearance of broad redox peaks and larger capacitive current. The positions of redox peaks are different in graphene/GC and NG/GC electrodes, which may be related to the involvement of different kinds of oxygen-containing functional groups. Since higher surface area gives higher overall capacitance [36,37], NG/GC electrodes are expected to possess higher surface area than graphene/GC electrode, as can be proved by larger capacitive current measured for NG/GC electrodes.

To investigate the ORR electrocatalytic activity of NG materials, LSVs were recorded on different rotating disk electrodes. Analogous to the case of NG-1/GC electrode (Fig. 4A), the current density of all electrodes increases with rotation rate. Comparison of LSVs obtained at different electrodes with a rotation rate of 800 rpm is shown in Fig. 4B. On GC electrode, two reduction steps both ascribed to two-electron reduction of O_2 to HO_2^- are observed, in which the process at potentials around −0.5 V is mediated by native active quinone-like groups with superoxide anion as intermediate, and the other is a direct two-electron reduction on GC surface [38]. The modification of graphene and NG materials on GC surface triggers larger current density and more than 100 mV positive shift of half-wave potential, and this is closely associated with the abundance of oxygen-containing functionalities and high surface area displayed in Fig. 3. On graphene/GC electrode, two reduction processes are also recorded, but there is a current plateau between −0.50 and −0.70 V. By comparison, NG/GC electrodes exhibit one single reduction step. The current density on NG-2/GC and NG-3/GC electrodes is larger than that on NG-1 and NG-4 modified ones, and NG-5/GC electrode possesses the lowest electrocatalytic activity. Since all NG/GC electrodes have similar surface areas as indicated by the capacitance current in Fig. 3, the chemical composition and microstructure of NG materials play quite an important role in electrochemical performance, which will have a great effect on conductivity, the activity, number and distribution of active sites. Here, ORR activity of graphene materials is not proportional to the total nitrogen content, which increases first and then decreases with a rise in nitrogen content. The incorporation of nitrogen brings new active sites and provides additional electrons to the aromatic π-system, but it increases structure defectiveness indicated by an increase in I_D/I_G values to lower the mobility of current carriers in the meanwhile [39], and an optimal value is expected to balance the advantages of nitrogen doping against its disadvantages. NG-2 and NG-3 possessing the highest activity give a nitrogen content of around 7% with an I_D/I_G value of ca. 1. If these values are smaller (NG-1), the active sites available are not enough, and larger ones (NG-4 and NG-5) will give poor conductivity. As for the role of different nitrogen species, no obvious dependence of ORR activity on the proportions of N1, N2, and N3 has been observed. Thus it is difficult to establish which type of nitrogen species should be responsible for the enhanced ORR electrocatalytic properties of NG materials. Furthermore, the performance of these NG materials towards ORR is still not as good as that of the commercial Pt/C in terms of the half-wave potential and current density.

For further insight into ORR mechanism on different electrodes, Koutechy–Levich (K–L) plots are constructed on the basis of LSVs according to K–L equation:

$$\frac{1}{i} = \frac{1}{i_k} + \frac{1}{0.62nFC_0D_0^{2/3}\nu^{-1/6}\omega^{1/2}}$$

where i is the measured current density, i_k is the kinetic current density, n is the number of electrons transferred per O_2 molecule, F is the Faraday constant (96485 C mol^{-1}), ω is the angular velocity of rotation, C_0 is the saturation concentration of O_2, D_0 is the O_2 diffusion coefficient, and ν is the kinematic viscosity of 0.1 M KOH. Fig. 5A and B depict K–L plots for different electrodes at −0.5 and −1.1 V, typical potentials for two reduction steps of ORR on bare GC and graphene/GC electrodes. All plots give good linearity, indicating first-order reaction kinetics for ORR with respect to the concentration of O_2 [40,41].

Based on slopes and intercepts of linear K–L plots, the values of n and i_k at different potentials on various electrodes can be obtained, which are shown in Fig. 5C and D. On bare GC electrode, the dependence curve of n on potential is divided into two steps corresponding to the reduction of O_2 to HO_2^- in two different ways. The values of n on graphene/GC electrode are around 2 at potentials more positive than −0.6 V, and then increase to ca. 4 rapidly. Therefore, the second process should be attributed to further reduction of HO_2^-, which is quite different from the case for GC electrode. The n values on all NG/GC electrodes are around 3 at lower overpotentials, demonstrating the coexistence of two- and four-electron reduction of O_2. A rise in overpotential provides more activation energy to favor four-electron ORR, and accordingly an increase of n values with potential negative shift is observed. Larger n values on NG/GC electrodes than those on graphene/GC electrode at lower overpotentials confirm superior electrocatalytic ORR properties caused by nitrogen doping. The incorporation of nitrogen polarizes the adjacent carbon atoms to enhance the adsorption of O_2 and to readily attract electrons for faciliating ORR [42]. In accordance with the results of LSVs, NG-5/GC electrode reveals the smllest n values among all NG modified electrodes. i_k reflects the intrinsic properties of electrode materials, and it can also provide information on reaction paths. The values of i_k on GC and graphene/GC electrodes increase first, and then decrease, and increase again with a fall in potential, but those on NG/GC electrodes increase smoothly, which results from different reaction mechanisms. The ORR on GC and graphene/GC electrodes consists of two individual steps, and a slight increase in overpotential gives more activation energy to the first reduction process, and consequently larger i_k values are expected. When overpotentials are moderate, the transition between two reduction steps occurs, and i_k gives smaller values for unfavorable kinetics of the second process. Further negative shift of potential favors the second reduction step, and i_k gives larger values again. The smooth increase of i_k values on NG/GC electrodes is attributed to no clear potential divisions between two- and four-electron reduction of O_2 and favorable four-electron reduction with the rise in overpotential.

4. Conclusions

NG materials with high nitrogen contents (>6%) synthesized via hydrothermal reaction of GO with urea possess good electrocatalytic activity towards ORR in 0.1 M KOH. At graphene modified GC electrode, ORR undergoes two successive two-electron processes with HO_2^- as intermediate. The incorporation of nitrogen increases the number of electrons transferred per O_2 molecular from ca. 2 of graphene to around 3 at lower overpotentials, indicating that the transformation of O_2 to OH^- occurs. The electrocatalytic properties of NG materials are closely related to their nitrogen contents and microstructure, which follow an order of NG-2 ≈ NG-3 > NG-1 ≈ NG-4 > NG-5. A defined amount of nitrogen is necessary for the enhancement of ORR activity, but an excess of nitrogen brings lager defect densities in microstructure that will have adverse effects.

Acknowledgments

This work was supported by the National Natural Science Foundation of China (No. 51131008), and Chinese Academy of Sciences (No. KZCX2-YW-205-03).

References

[1] Q.G. He, X.F. Yang, X.M. Ren, B.E. Koel, N. Ramaswamy, S. Mukerjee, R. Kostecki, Journal of Power Sources 196 (2011) 7404–7410.
[2] X.G. Li, B.N. Popov, T. Kawahara, H. Yanagi, Journal of Power Sources 196 (2011) 1717–1722.
[3] M. Mamlouk, S.M.S. Kumar, P. Gouerec, K. Scott, Journal of Power Sources 196 (2011) 7594–7600.
[4] B.B. Blizanac, P.N. Ross, N.M. Markovic, Electrochimica Acta 52 (2007) 2264–2271.
[5] D. Zhang, D.H. Chi, T. Okajima, T. Ohsaka, Electrochimica Acta 52 (2007) 5400–5406.
[6] Y. Wang, D. Zhang, H.Q. Liu, Journal of Power Sources 195 (2010) 3135–3139.
[7] D.Y. Qu, Carbon 45 (2007) 1296–1301.
[8] L.H. Tang, Y. Wang, Y.M. Li, H.B. Feng, J. Lu, J.H. Li, Advanced Functional Materials 19 (2009) 2782–2789.
[9] Y.Y. Liang, Y.G. Li, H.L. Wang, J.G. Zhou, J. Wang, T. Regier, H.J. Dai, Nature Materials 10 (2011) 780–786.
[10] J.J. Wu, D. Zhang, Y. Wang, Y. Wan, B.R. Hou, Journal of Power Sources 198 (2012) 122–126.
[11] J.J. Wu, D. Zhang, Y. Wang, Y. Wan, Electrochimica Acta 75 (2012) 305–310.
[12] S.Y. Wang, L.P. Zhang, Z.H. Xia, A. Roy, D.W. Chang, J.B. Baek, L.M. Dai, Angewandte Chemie International Edition 51 (2012) 4209–4212.
[13] L.T. Qu, Y. Liu, J.B. Baek, L.M. Dai, ACS Nano 4 (2010) 1321–1326.
[14] S.B. Yang, L.J. Zhi, K. Tang, X.L. Feng, J. Maier, K. Müllen, Advanced Functional Materials (2012). http://dx.doi.org/10.1002/adfm.201200186.
[15] Z.H. Sheng, L. Shao, J.J. Chen, W.J. Bao, F.B. Wang, X.H. Xia, ACS Nano 5 (2011) 4350–4358.
[16] Z.Q. Luo, S.H. Lim, Z.Q. Tian, J.Z. Shang, L.F. Lai, B. MacDonald, C. Fu, Z.X. Shen, T. Yu, J.Y. Lin, Journal of Materials Chemistry 21 (2011) 8038–8044.
[17] D.S. Geng, Y. Chen, Y.G. Chen, Y.L. Li, R.Y. Li, X.L. Sun, S.Y. Ye, S. Knights, Energy & Environmental Science 4 (2011) 760–764.
[18] D.C. Wei, Y.Q. Liu, Y. Wang, H.L. Zhang, L.P. Huang, G. Yu, Nano Letters 9 (2009) 1752–1758.
[19] Y. Wang, Y.Y. Shao, D.W. Matson, J.H. Li, Y.H. Lin, ACS Nano 4 (2010) 1790–1798.
[20] K.S. Subrahmanyam, L.S. Panchakarla, A. Govindaraj, C.N.R. Rao, Journal of Physical Chemistry C 113 (2009) 4257–4259.
[21] X.L. Li, H.L. Wang, J.T. Robinson, H. Sanchez, G. Diankov, H.J. Dai, Journal of American Chemical Society 131 (2009) 15939–15944.
[22] S.A. Hasan, E.K. Tsekoura, V. Sternhagen, M. Stromme, Journal of Physical Chemistry C 116 (2012) 6530–6536.
[23] L. Sun, L. Wang, C.G. Tian, T.X. Tan, Y. Xie, K.Y. Shi, M.T. Li, H.G. Fu, RSC Advances 2 (2012) 4498–4506.
[24] D.H. Long, W. Li, L.C. Ling, J. Miyawaki, I. Mochida, S.H. Yoon, Langmuir 26 (2010) 16096–16102.
[25] Y.J. Zhang, K. Fugane, T. Mori, L. Niu, J.H. Ye, Journal of Materials Chemistry 22 (2012) 6575–6580.
[26] G.X. Wang, X.P. Shen, B. Wang, J. Yao, J. Park, Carbon 47 (2009) 1359–1364.
[27] X.B. Fan, W.C. Peng, Y. Li, X.Y. Li, S.L. Wang, G.L. Zhang, F.B. Zhang, Advanced Materials 20 (2008) 4490–4493.
[28] L.Y. Feng, Y.G. Chen, L. Chen, ACS Nano 5 (2011) 9611–9618.
[29] G.X. Ma, R.R. Jia, J.H. Zhao, Z.J. Wang, C. Song, S.P. Jia, Z.P. Zhu, Journal of Physical Chemistry C 115 (2011) 25148–25154.
[30] C.V. Rao, Y. Ishikawa, Journal of Physical Chemistry C 116 (2012) 4340–4346.
[31] Y.Y. Shao, S. Zhang, M.H. Engelhard, G.S. Li, G.C. Shao, Y. Wang, J. Liu, I.A. Aksay, Y.H. Lin, Journal of Materials Chemistry 20 (2010) 7491–7496.
[32] S. Kundu, T.C. Nagaiah, W. Xia, Y.M. Wang, S. Van Dommele, J.H. Bitter, M. Santa, G. Grundmeier, M. Bron, W. Schuhmann, M. Muhler, Journal of Physical Chemistry C 113 (2009) 14302–14310.
[33] A. Kumar, A. Ganguly, P. Papakonstantinou, Journal of Physics: Condensed Matter 24 (2012) 235503–235508.
[34] A.C. Ferrari, J.C. Meyer, V. Scardaci, C. Casiraghi, M. Lazzeri, F. Mauri, S. Piscanec, D. Jiang, K.S. Novoselov, S. Roth, A.K. Geim, Physical Review Letters 97 (2006) 187401–187404.
[35] Z.H. Ni, T. Yu, Y.H. Lu, Y.Y. Wang, Y.P. Feng, Z.X. Shen, ACS Nano 2 (2008) 2301–2305.
[36] S. Maldonado, K.J. Stevenson, Journal of Physical Chemistry B 108 (2004) 11375–11383.
[37] X.H. Kang, J. Wang, H. Wu, I.A. Aksay, J. Liu, Y.H. Lin, Biosensors and Bioelectronics 25 (2009) 901–905.
[38] K. Tammeveski, K. Kontturi, R.J. Nichols, R.J. Potter, D.J. Schiffrin, Journal of Electroanalytical Chemistry 515 (2001) 101–112.
[39] Z.R. Ismagilov, A.E. Shalagina, O.Y. Podyacheva, A.V. Ischenko, L.S. Kibis, A.I. Boronin, Y.A. Chesalov, D.I. Kochubey, A.I. Romanenko, O.B. Anikeeva, T.I. Buryakov, E.N. Tkachev, Carbon 47 (2009) 1922–1929.
[40] I. Jiang, G.M. Brisard, Electrochimica Acta 52 (2007) 4487–4496.
[41] N.R. Elezovic, B.M. Babic, L. Gajic-Krstajic, V. Radmilovic, N.V. Krstajic, L.J. Vracar, Journal of Power Sources 195 (2010) 3961–3968.
[42] K.P. Gong, F. Du, Z.H. Xia, M. Durstock, L.M. Dai, Science 323 (2009) 760–764.